Ann. Rev. Astron. Astrophys. 1983. 21: 239–70

INTERSTELLAR AMMONIA

Paul T. P. Ho

Department of Astronomy, Harvard University, Cambridge, Massachusetts 02138

Charles H. Townes

Department of Physics, University of California, Berkeley, California 94720

1. BACKGROUND

Ammonia (NH_3) was the first polyatomic molecule detected in interstellar space, and since its initial discovery by Cheung et al. (1968), NH_3 has proved to be an invaluable spectroscopic tool in the study of the interstellar medium. Because of its large number of transitions sensitive to a wide range of excitation conditions and the fact that it can be detected in a great variety of regions, NH_3 is perhaps second only to carbon monoxide (CO) in importance.

1.1 *Physics of the Molecule*

The pyramidal NH_3 molecule is the classic example of a symmetric top with inversion, and is therefore well understood in laboratory microwave spectroscopy (Townes & Schawlow 1955, Kukolich 1967). Several important properties make NH_3 particularly interesting in astrophysical conditions. These are the existence of metastable and nonmetastable states, ortho- and para- species, inversion motion of the molecule, and hyperfine structures. We discuss these properties briefly.

The rotational energy of NH_3 is a function of the two principal quantum numbers (J, K), corresponding to the total angular momentum and its projection along the molecular axis. Unless there is some excitation of vibration transverse to the axis, the molecule has an electric dipole moment only along the molecular axis, and the dipole selection rules are $\Delta K = 0$, $\Delta J = 0, \pm 1$. Hence, dipole transitions between K-ladders (states with the

0066–4146/83/0915–0239$02.00

same value of K) are normally forbidden. Interaction between rotational and vibrational motions, even in the lowest vibrational state, induces a small dipole moment perpendicular to the rotation axis, giving rise to very slow $\Delta k = \pm 3$ ($K = |k|$) transitions (Oka et al. 1971); except for this, the K-ladders are essentially independent of each other. Normal intermolecular collisions (not involving weak magnetic effects) also produce only transitions in which Δk is a multiple of 3 (including 0). Within each K-ladder, the upper states ($J > K$) are called *nonmetastable* because they can decay rapidly (10–10^2 s) via the far-infrared $\Delta J = 1$ transitions. The lowest states can only decay via the much slower (10^9 s) $\Delta k = \pm 3$ transitions and are called *metastable*. It is clear that the nonmetastable states will be difficult to populate under normal astrophysical conditions, while the metastable states can be populated via $\Delta k = 3$ collisions. This is, in fact, substantiated by observations.

Because of the possible orientations of the hydrogen spins, two distinct species of NH_3 exist. These are ortho-NH_3 ($K = 3n$, n an integer, all H spins parallel) and para-NH_3 ($K \neq 3n$, all H spins not parallel). Since normal radiative and collisional transitions do not change the spin orientations, transitions between ortho- and para-NH_3 are also forbidden. (Note that $\Delta k = 3$ transitions will not mix the two species.) Various means to mix ortho- and para- species have been proposed by Cheung et al. (1969) with rather slow (10^{-6} yr^{-1}) rates. This leads to the suggestion that a rotational temperature between ortho- and para-NH_3 may reflect conditions at an earlier time, while a rotational temperature within the same species may reflect more recent conditions.

In addition to rotation, the NH_3 molecule also undergoes vibrational motion. In particular, the N atom can tunnel quantum mechanically through the plane of the H atoms. In contrast to most nonplanar molecules, the potential barrier due to the H atoms is low enough that such tunneling occurs rapidly, resulting in the two lowest vibrational states providing a transition frequency that falls in the microwave range. All (J, K) rotational states are thus split into inversion doublets (except for $K = 0$, where nuclear spin statistics and symmetry considerations eliminate half of the inversion doublet). The $\Delta J = 0$, $\Delta K = 0$ inversion transitions across the doublets are allowed from symmetry considerations (Townes & Schawlow 1955). Observations of these inversion transitions, in fact, constitute the bulk of our information on interstellar NH_3. Figure 1 gives an energy diagram of the rotation-inversion energy levels of NH_3.

The inversion doublets are further split by hyperfine interactions. The major effect is due to the interaction between the electric quadrupole moment of the N nucleus and the electric field of the electrons. Since the ^{14}N spin is unity, each level of the doublet is split by the nuclear orientation into

3 hyperfine states, resulting in 5 distinct components of the transition frequency. These are a main line ($\Delta F_1 = 0$, $\mathbf{F}_1 = \mathbf{J} + \mathbf{I}_N$, where $\mathbf{I}_N$ is the nitrogen spin) having at least 50% of the total intensity, and two pairs of satellite lines ($\Delta F_1 = \pm 1$) with roughly equal intensities, separated from the main line by ~ 1 MHz. Weaker magnetic interactions due to $\mathbf{I}_N \cdot \mathbf{J}$ and $\mathbf{I} \cdot \mathbf{J}$ couplings ($\mathbf{I}$ is the sum of H spins), as well as H-N and H-H spin-spin interactions, introduce further splittings on the order of ~ 40 kHz. For the $(J, K) = (1, 1)$ transition, a total of 18 distinct hyperfine components are obtained. Figure 2 shows the hyperfine structure of this transition. For typical molecular clouds in the Galaxy, the electric quadrupole hyperfine structure of the lower metastable states, e.g. (1, 1) and (2, 2), can be detected easily (cf. Barrett et al. 1977). For quiescent nearby dark clouds, even the magnetic hyperfine structures have been resolved (cf. Ho et al. 1977, Rydbeck et al. 1977). Figure 3 shows a spectrum of the (1, 1) line toward L1498 (Myers & Benson 1983), where both quadrupole and magnetic hyperfine components can be seen. The great advantage of the hyperfine structure is that it allows us to deduce the optical depth of the transition. This circumvents the usual difficulties associated with determining optical

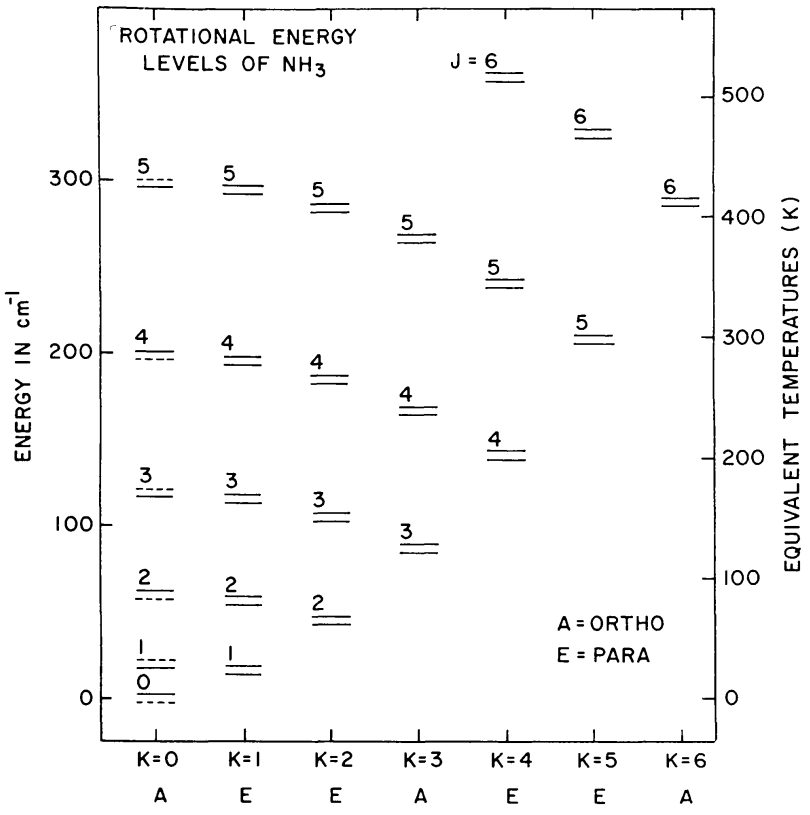

Figure 1 Energy level diagram of rotation-inversion states. J is the total angular-momentum quantum number, and K is the projected angular momentum along the molecular axis.

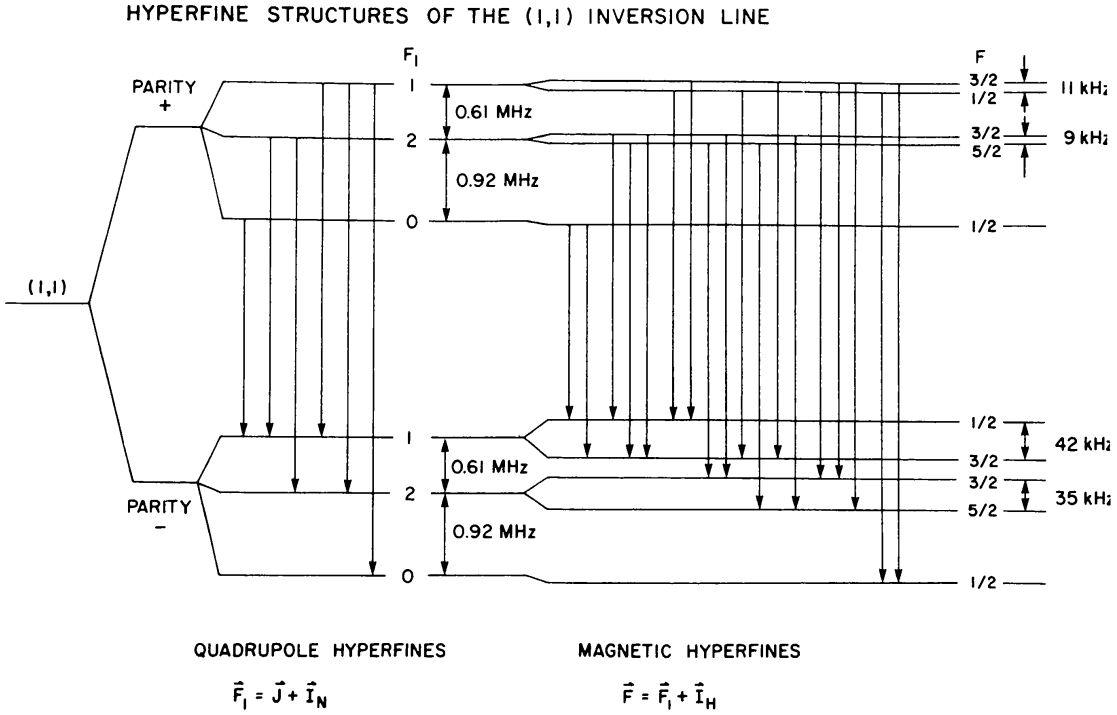

Figure 2 Hyperfine splitting of the $(J, K) = (1, 1)$ transition. The allowed transitions are indicated.

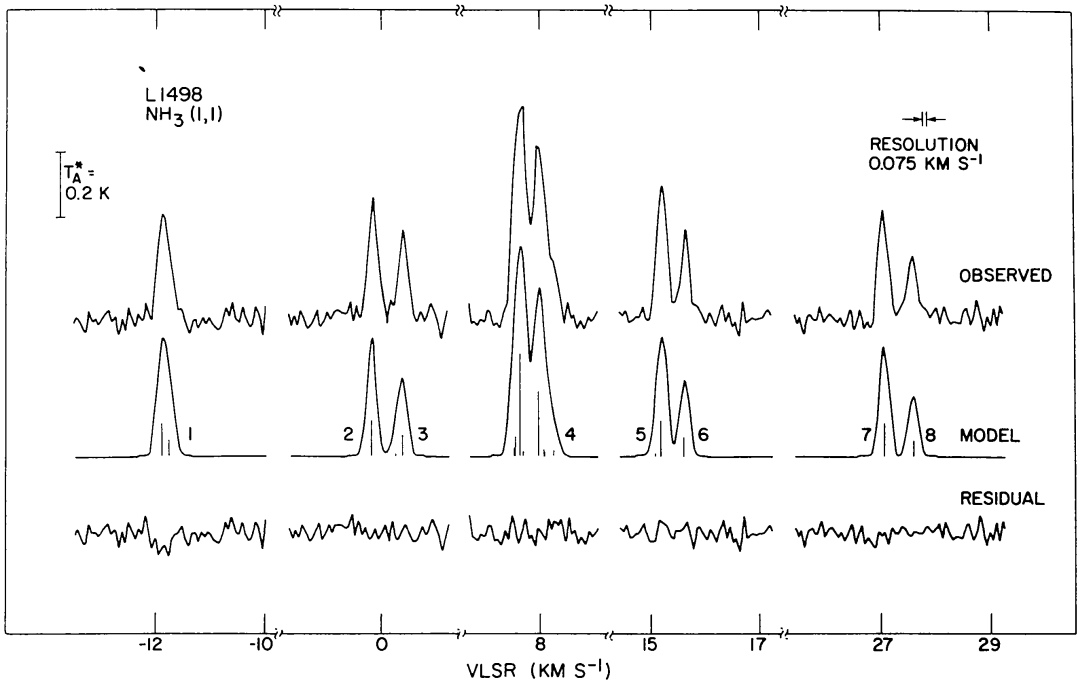

Figure 3 Observed $(J, K) = (1, 1)$ spectrum toward L1498 (Myers & Benson 1983). The relative LTE strengths of the various hyperfine components are indicated by the vertical tick marks under the model spectrum.

depth from isotopic studies, namely calibration over different frequency bands and the adoption of an isotopic ratio.

1.2 *Interstellar Excitation*

At the low temperature (10–10^2 K) of the interstellar medium, excitation of molecular transitions occurs mostly via collisions with molecular hydrogen (H_2). In fact, detection of NH_3 inversion emission in interstellar clouds provided the first clear evidence that many of these clouds had H_2 densities as high as about 10^3 cm^{-3} (Cheung et al. 1968). Whether a particular transition will reach thermodynamic equilibrium with its local surroundings depends on the competition between collisions and spontaneous radiative decays out of the upper levels. The advantage of the NH_3 molecule is the range in Einstein A coefficients covered by its many transitions. Table 1 lists the values of A for some of the detected transitions. For a typical collision cross section of $\sigma \sim 10^{-15}$ cm^2 (Green 1980) and gas temperatures of 10–10^2 K, the collision rate is $C \sim 4$–11×10^{-6} s^{-1} $[n(H_2)/10^5$ cm$^{-3}]$. It is clear that collisions will dominate the excitation of the lower metastable inversion doublets, while densities on the order of 10^8–10^9 cm^{-3} will be required to populate the nonmetastable levels. Although radiative-trapping effects will help in exciting the typically optically thick far-infrared transitions, it is likely that both radiation and very high densities are important in these cases. Transitions in the rotation-vibration bands have the shortest radiative lifetimes and consequently have been detected to date only in nearby dense circumstellar envelopes (Betz et al. 1979), and even there mostly in absorption.

Table 1 Einstein A coefficients

Transition[a]	Frequency (Hz)	Energy[b] (K)	Einstein A (s^{-1})
(4, 2)	21.703358×10^9	265.1	5.13×10^{-8}
(2, 1)	23.098819×10^9	80.6	5.15×10^{-8}
(3, 2)	22.834185×10^9	150.7	9.95×10^{-8}
(4, 3)	22.688312×10^9	239.0	1.32×10^{-7}
(1, 1)	23.694495×10^9	23.4	1.67×10^{-7}
(2, 2)	23.722633×10^9	64.9	2.23×10^{-7}
(9, 8)	23.657471×10^9	952.4	2.36×10^{-7}
(3, 3)	23.870129×10^9	124.5	2.56×10^{-7}
(6, 6)	25.056025×10^9	412.4	3.38×10^{-7}
$(4, 3)^a \rightarrow (3, 3)^s$	24.051244×10^{11}	239.0	6.79×10^{-2}
(1, 0) → (0, 0)	57.249815×10^{10}	28.6	1.57×10^{-3}

[a] All are inversion transitions except for the last two entries, which are rotational transitions.

[b] Energy above ground state in equivalent temperatures.

1.3 *Formation and Dissociation Mechanisms*

The interstellar abundance of NH_3 has been measured for a variety of regions. The $[NH_3]/[H_2]$ ratio has been estimated to range from 10^{-7} in small dark clouds (cf. Ungerechts et al. 1980) up to 10^{-5} in the dense core of the Orion molecular cloud (Genzel et al. 1982). Ion-molecule chemistry (Prasad & Huntress 1980, Mitchell et al. 1978, Herbst & Klemperer 1973) can produce abundances on the order of 10^{-8} at densities $n(H_2) \sim 10^5$ cm^{-3}.

The principal formation mechanism generally proposed for interstellar NH_3 is the reaction

$$NH_4^+ + e^- \rightarrow NH_3 + H.$$

The principal dissociation mechanisms are

$$HCO^+ + NH_3 \rightarrow NH_4^+ + CO,$$

$$H_3^+ + NH_3 \rightarrow NH_4^+ + H_2,$$

$$H_3^+ + NH_3 \rightarrow NH_3^+ + H_2 + H.$$

These reactions are often temperature dependent. For example, the production of NH_4^+ via $NH_3^+ + H_2 \rightarrow NH_4^+ + H$ has a rising exponential dependence on T for $T > 100$ K (Fehsenfeld et al. 1975). Dalgarno (1982), however, reports that the rate coefficients may rise again at low temperatures, so that synthesis of NH_3 may be enhanced at the 10–20 K temperature in dark clouds. The radiative association reactions

$$NH_3^+ + H_2 \rightarrow NH_3^+ \cdot H_2 + h\nu,$$

$$NH_3^+ \cdot H_2 + e^- \rightarrow NH_3 + H_2,$$

have also been suggested to be important at low temperatures. The consensus then is that the abundance in low-temperature dark clouds should be achievable via ion-molecule chemistry. The situation in very dense and warm cores, as in Orion, is more problematical, since the warmer temperatures will slow down the reaction rates and ions are collisionally depleted at higher densities.

In view of the enhanced abundances in denser regions, it is possible that grain chemistry is important. Evaporation or sputtering off grains due to the higher temperatures and collision rates may release NH_3 from the grain surfaces (cf. Sweitzer 1978).

1.4 *The Ubiquitous NH_3 Molecule*

Because of the abundance of transitions that sample a large area in the density-temperature plane, NH_3 can be detected easily in quiescent dark clouds (Ho et al. 1978, Ungerechts et al. 1980) and regions of active low-

luminosity star formation (Ho & Barrett 1980, Lang & Willson 1980), as well as regions of high-luminosity star formation (Ho et al. 1981). NH_3 has been detected also in circumstellar envelopes (Betz et al. 1979, McLaren & Betz 1980), in planetary atmospheres (Greenberg et al. 1977), and in external galaxies (Martin & Ho 1979, Martin et al. 1982). Essentially all types of regions containing molecular material can be studied with an appropriate choice of NH_3 transitions.

With the recent completion of the Very Large Array (VLA) in New Mexico, the NH_3 inversion lines at $\lambda \sim 1$ cm have taken on a new importance. At the high-frequency end of the current operating range of the VLA, the achieved angular resolution of $<1''$ is the best available for spectral line studies for some time to come, except, of course, for VLBI work on the special and intense sources that are masing. Distant molecular regions can be studied with good spatial resolution (<0.05 pc at 10 kpc distance) for the first time.

2. OBSERVING TECHNIQUES AND INSTRUMENTS

2.1 *Single-Antenna Facilities*

At $\lambda \sim 1$ cm, several large telescopes are available for NH_3 studies throughout the world, both in the Northern and Southern Hemispheres. These include the 100-m Effelsberg telescope in Germany (Wilson et al. 1979), the 20-m Onsala telescope in Sweden (Rydbeck et al. 1977), the 25-m Chilbolton telescope in England (Macdonald et al. 1981, Little et al. 1977), the 46-m Algonquin telescope in Canada (Kwok et al. 1981), the 37-m Haystack telescope (Barrett et al. 1977) and the 43-m Green Bank telescope (Morris et al. 1973) in the United States, the 14-m Itapetinga telescope in Brazil (Scalise et al. 1981), the inner 17 m of the Parkes telescope (Batchelor et al. 1977), and the 64-m NASA-JPL Deep Space Network telescope (Dickinson et al. 1982) in Australia. Despite the intrinsic low-brightness temperature of most NH_3 lines due to modest optical depths and clumping effects (see Section 4.2), studies are made possible as most of these telescopes are equipped with maser preamplifiers (e.g. Moore & Clauss 1979). System temperatures on the sky are typically <100 K. This means that typical NH_3 lines in nearby dark clouds can be detected with ~ 1 km s^{-1} spectral resolution by ~ 10 minutes of integration. Hence, sensitivity of single-antenna NH_3 studies is only a factor of a few less than for CO studies.

2.2 *Interferometric Studies with the Very Large Array*

At cm and mm wavelengths, single-antenna studies provide typical angular resolution on the order of $\sim 1'$. To achieve arcsec resolution, aperture synthesis techniques are required. For some time, VLBI techniques have been usable on intense molecular sources such as H_2O masers. However,

the combined effect of high angular resolution and limited antenna area has not allowed useful work of this type on nonmaser sources. With the completion of the Very Large Array (Thompson et al. 1980) of the National Radio Astronomy Observatory, up to twenty-seven 25-m antennas can be linked together with projected baselines of 40 m up to 36 km. Even in the most compact D configuration (maximum baseline 1.0 km), the angular resolution at $\lambda \sim 1$ cm is $\sim 3''$. This is already the best that can be achieved for molecular line studies in the radio regime, better than the resolution achieved with millimeter-wave interferometry at the Hat Creek Observatory (Plambeck et al. 1982). The total collecting area of the VLA is equivalent to that of a 130-m antenna. With the development of cooled FET amplifiers (Weinreb 1980), the next generation of VLA *K*-band receivers should be nearly as sensitive as maser receivers. At that point, the primary limiting factor for aperture synthesis will be phase instabilities of the atmosphere at $\lambda \sim 1$ cm. This can be circumvented by using favorable atmospheric conditions, by phase closure techniques, or by adaptive calibration involving successive self-consistent corrections of a model (Schwab 1980).

2.3 *Infrared and Submillimeter Techniques*

Fundamental vibrational bands of NH_3 occur near 3-μm, 6-μm, and 10-μm wavelengths. For these, optical telescopes are used, although only the 3-μm and 10-μm regions can be studied from the ground because of atmospheric opacity. A moderately broad band at 2.97 μm attributed to solid NH_3 has been detected toward Orion with a spectrometer using a circular variable filter and a InSb photoconductive detector (Knacke et al. 1982).

While any broad absorption near 10 μm due to solid NH_3 is characteristically obscured by silicate dust absorption, the narrow vibrational lines of gaseous NH_3 in the 10-μm atmospheric window have been observed. In planetary atmospheres, spectrometers of moderately high resolution, such as the grating, Fabry-Perot, or Fourier transform systems, are useful. For detection of NH_3 in circumstellar material, the very high resolution of a heterodyne spectrometer, using a HgCdTe photodiode mixer and a CO_2 local oscillator, has been especially effective (Betz et al. 1977, Betz et al. 1979). The angular field of view in this case corresponds to the diffraction beam width of large telescopes (1–3″). Detections are typically in absorption against the continuum of stellar disks or circumstellar dust shells; P Cygni line shapes are seen in some cases. The effective angular resolution in absorption is usually defined by the size of the continuum source, which is smaller than the beam width.

For the rotational transitions of NH_3 in the far-infrared, the atmosphere is essentially opaque. Observations are therefore obtained with the 0.9-m telescope on the NASA Kuiper Airborne Observatory at typical altitudes of

12 km. The receivers are photoconductive detectors, and the spectrometer involves two tandem Fabry-Perot interferometers, with parts of the system cooled to liquid-helium temperatures (Storey et al. 1980). The angular resolution at 125 μm is $\sim 44''$ and spectral resolution is typically ~ 75–90 km $^{-1}$ (Townes et al. 1983).

The ground state $(1,0) \rightarrow (0,0)$ rotational transition occurs at 524 μm. Again, because of the atmosphere, observations must be conducted from the Kuiper Airborne Observatory. The receiver used at this submillimeter wavelength was an InSb hot-electron bolometer as described by Phillips & Jefferts (1974). The angular resolution was $2'$. Although the intrinsic bandwidth of the device was 1 MHz, sweeping of the local oscillator provided a larger spectral window with an effective resolution of ~ 2 km s^{-1} (Keene et al. 1983).

3. ANALYSIS OF THE SPECTRAL DATA

We emphasize the $\lambda \sim 1$ cm inversion lines because the best spectral resolutions and most extensive data are obtained at present with these transitions.

3.1 *Derivation of Optical Depths*

For the lowest metastable inversion lines, the hyperfine structures can be detected and resolved. Since the relative intensities for the various hyperfine transitions are known (cf. Townes & Schawlow 1955), the optical depths of the transition can be derived from the observed relative brightness temperatures of the different hyperfine components. For the electric quadrupole hyperfine structure of the (J,K) inversion line, one obtains (Mayer et al. 1973, Barrett et al. 1977),

$$\frac{\Delta T_a^*(J,K,m)}{\Delta T_a^*(J,K,s)} = \frac{1-e^{-\tau(J,K,m)}}{1-e^{-a\tau(J,K,m)}}, \qquad 1.$$

where ΔT_a^* is the observed brightness temperature, m and s refer to the main and satellite hyperfine components, $\tau(J,K,m)$ is the optical depth of the main component, and a is the ratio of the intensity for the satellite compared with the main component [$a = 0.28$ and 0.22 for the $(1,1)$ satellites]. Hence, $\tau(J,K,m)$ can be derived numerically from the ratio of ΔT_a^* values. Note that Equation 1 assumes equal beam-filling factors and excitation temperatures for the different hyperfine components. This is reasonable because of the very close energy separations and the small probability of special excitation mechanisms that differentiate between the hyperfine components.

Two other methods for deducing the optical depths are absorption studies and isotopic studies. A comparison of the absorption line strengths

and the continuum gives a lower limit to the optical depth (Ho & Barrett 1978a, Pauls & Wilson 1980). It is a lower limit because the line-absorption region may not cover the entire background continuum region. The $^{15}NH_3$ $(J, K) = (1, 1)$ isotopic line has been detected toward Orion (Wilson & Pauls 1979). Detection of the rarer N isotope is difficult because the terrestrial $[^{15}N]/[^{14}N]$ ratio is 1/273. The vastly different optical depths may also complicate the interpretation, as the beam-filling factors may be very different. Deuterated ammonia (NH_2D) has also been detected (Turner et al. 1978). However, because of the very different frequencies of the isotopic lines and the unknown excitation temperature of NH_2D, the derivation of optical depths is uncertain.

3.2 *Excitation Measurements*

With the derivation of optical depth, the product $\eta_b[J_\nu(T_{ex}) - J_\nu(T_b)]$ is deduced (Barrett et al. 1977), where η_b is the beam-filling factor, $J_\nu(T) = (h_\nu/k)[e^{h\nu/kT} - 1]^{-1}$ is the Rayleigh-Jeans temperature, and T_{ex} and T_b are the excitation and background temperatures. If the beam is uniformly filled, $\eta_b = 1$, and T_{ex} for the transition can be derived directly.

Because transitions between the metastable inversion doublets are usually much faster than those to other rotational states, they can be approximated as a two-level system. By balancing collisions and stimulated emission against spontaneous emission, one obtains a relation between the density and the excitation temperature

$$n(H_2) = \frac{A}{C}\left[\frac{J_\nu(T_{ex}) - J_\nu(T_b)}{J_\nu(T_k) - J_\nu(T_{ex})}\right]\left[1 + \frac{J_\nu(T_k)}{h\nu/k}\right], \qquad 2.$$

where A and C are the Einstein A coefficient and the collision rate, respectively, and T_k is the gas kinetic temperature. Hence, once T_{ex} and T_k are determined, $n(H_2)$ can be calculated, and vice versa. Of course if the density and temperature are high enough that the upper nonmetastable states become populated, multilevel statistical equilibrium calculations (Sweitzer 1978) will be required. The basic premise remains true in that $n(H_2)$ and T_{ex} are directly related.

By observing several NH_3 transitions, it is possible to calculate a rotational temperature characterizing the distribution of population among the different energy states (Ho et al. 1979):

$$\frac{\tau(J', K')}{\tau(J, K)} = \frac{\nu^2(J', K')}{\nu^2(J, K)} \frac{\Delta\nu(J, K)}{\Delta\nu(J', K')} \frac{T_{ex}(J, K)}{T_{ex}(J', K')} \frac{|\mu(J', K')|^2}{|\mu(J, K)|^2} \frac{g(J', K')}{g(J, K)} \times \exp\left\{\frac{-\Delta E(J', K'; J, K)}{kT_R(J', K'; J, K)}\right\}, \qquad 3.$$

where $|\mu(J,K)|^2 = \mu^2 K^2/[J(J+1)]$ are the dipole matrix elements, g is the statistical weight, and ΔE and T_R are the energy difference and rotational temperature, respectively, between the two states. In the case where the lower state is the (1, 1) state so that $\tau(1,1,m)$ can be measured, $\tau(J,K)$ can be deduced from the ratio of the observed brightness temperatures ΔT_a^*, as in Equation 1. One can then solve directly for T_R, obtaining, for example,

$$T_R(2,2;1,1) = -41.5 \div \ln\left[\frac{-0.282}{\tau_m(1,1)} \ln\left\{1 - \frac{\Delta T_a^*(2,2,m)}{\Delta T_a^*(1,1,m)} \times (1 - e^{-\tau_m(1,1)})\right\}\right]. \quad 4.$$

Figure 4 shows the solution for $T_R(J',K';1,1)$ in the optically thin limit and the solution for $T_R(2,2;1,1)$ for different values of $\tau(1,1,m)$. This figure demonstrates that states with greater energy differences are better indicators of the higher-temperature regimes.

As discussed earlier, because of the downward relaxation of the nonmetastable states and the slow collisional coupling between K-ladders,

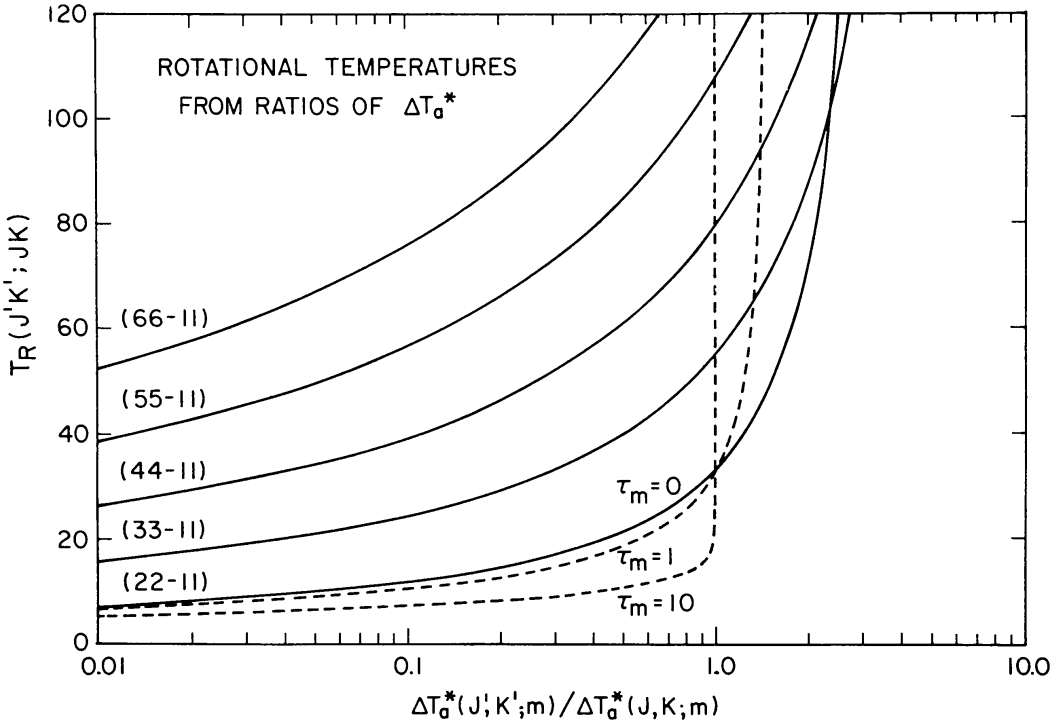

Figure 4 Calculated rotational temperatures from the ratio of intensities of metastable transitions. $\Delta T_a^*(J,K;m)$ denotes the brightness temperature of the main quadrupole hyperfine component. The effect of optical depths is shown for the rotational temperature between the (2, 2) and (1, 1) states. τ_m is the optical depth of the main quadrupole hyperfine of the (1, 1) line. $\tau_m = 0$ corresponds to the optically thin case.

the metastable populations may not resemble a true Boltzmann distribution. Nevertheless, as shown by Figure 5, T_R is a good indicator of the gas temperature T_k as deduced from CO, with similar angular resolutions toward a variety of regions (Martin et al. 1982). Although T_R underestimates T_k, the good empirical correlation between the two quantities demonstrates that T_R is a reliable indicator. Walmsley & Ungerechts (1983) have performed statistical equilibrium calculations demonstrating that, after corrections for the depopulation effect, the NH_3 and CO temperatures are in good agreement.

These considerations demonstrate that by measuring two or more transitions of the NH_3 molecule, one can determine in a self-consistent manner the density and temperature of the ambient molecular material.

3.3 *Ortho-Para Measurements*

Early studies (Cheung et al. 1969, Morris et al. 1973) indicated that deduced values of T_R between ortho- and para- species often disagreed with values

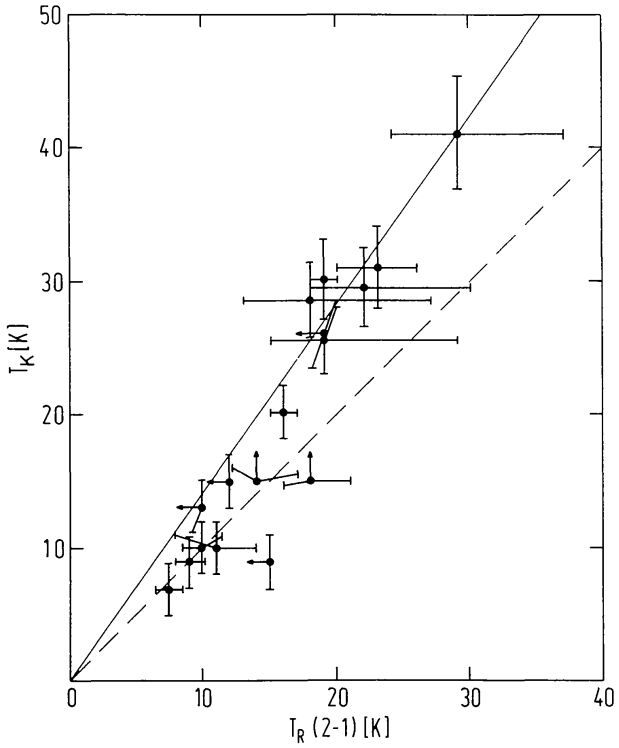

Figure 5 Empirical correlation between rotational temperatures deduced from NH_3 observations of the $(J, K) = (1, 1)$ and $(2, 2)$ lines and the gas kinetic temperature deduced from CO observations (Martin et al. 1982). Both data sets refer to comparable angular resolutions. The solid and dashed lines indicate that T_R underestimates T_k especially in the higher-temperature regions.

deduced within the same species. This has led to speculations of anomalous ortho-para abundance ratios and nonequilibrium population distributions. More recent measurements (cf. Barrett et al. 1977) suggest that these anomalies may be due to beam-filling factors associated with small-scale structures, and the resulting imperfect determination of optical depths. The presence of both absorption and emission within the same beam (Winnewisser et al. 1979, Pauls & Wilson 1980) and the blending of several velocity features (Ho & Barrett 1978b) also complicate the analysis. Indeed, the recent measurement of several NH_3 lines in absorption and emission toward W33 (Wilson et al. 1982) suggests that a small amount of non-LTE excitation for one of the transitions could prevent the reliable determination of an ortho-para ratio. In view of the various difficulties, the solution to the ortho-para problem awaits high angular and spectral resolution measurements with good sensitivity that will fully resolve the emission and/or absorption structures.

3.4 *Cross Sections*

Using microwave double-resonance techniques, Oka (1968a,b) measured the strengths of collision-induced transitions between various rotational states. However, since the laboratory measurements were performed at standard conditions, the results must be extrapolated to the low temperature of the interstellar medium (cf. Schwartz 1979, Matsakis et al. 1980). The best available cross sections are probably those due to *ab initio* quantum mechanical calculations by Green (1980, 1981), which use Hartree-Fock treatment for short-range forces and a model for long-range forces including a spherical R^{-6} term and a quadrupole-induced dipole term. For NH_3-H_2 collisions where H_2 is in the para-state and $T_k = 15$ K, the cross section for the (1, 1) inversion doublet is equivalent to a hard sphere value of $\sim 3 \times 10^{-15}$ cm^2. The cross sections for the inversion transitions are in general an order of magnitude higher than the cross sections to any other state. This confirms that a two-level treatment is adequate for the modest density and temperature regimes. However, a full multilevel treatment will be required for higher excitation regimes.

4. MAJOR OBSERVATIONAL RESULTS

Significant progress has been made in the past decade in our understanding of the properties and evolution of the interstellar medium. The study of the NH_3 molecule has illuminated a number of topics, which are described below. With the successful application of interferometric and far-infrared techniques, even greater advances will be made in the next few years.

4.1 *Observations of Nearby Dark Clouds*

The detection of the $(J, K) = (1, 1)$ inversion line of NH_3 in cool nearby dark clouds was first reported by Morris et al. (1973) and Cheung et al. (1973). It was clear from the beginning that these clouds represent an important class of objects because they are close to us, typically ~ 100 pc. With the angular resolution ($\sim 1'$) of single antennas, spatial resolution of 0.03 pc was readily available. Later observations by Ho et al. (1977) and Rydbeck et al. (1977) with finer spectral resolution revealed that these cool dark clouds tend to be rather quiescent regions with intrinsic line widths of ~ 0.3 km s^{-1}, after corrections for hyperfine broadening. Detection of the many hyperfine components due to quadrupole and magnetic interactions for the (1, 1) inversion doublet (see Section 1.1 and Figure 2) enabled an accurate determination of the line width, emission velocity, and optical depth. A subsequent survey of a large number of dark clouds (Ho et al. 1978) confirmed the prevalent narrow line widths. Since the velocity width contribution from thermal motion alone is 0.16 km s^{-1} at a gas temperature of 10 K, it is clear that any turbulent or systematic motion must be relatively small and essentially sonic or subsonic in these dark clouds. With improvements in sensitivity, Ungerechts et al. (1980) and Myers & Benson (1980) succeeded in detecting the $(J, K) = (2, 2)$ line in a number of dark clouds. A comparison with the (1, 1) line intensity indicates a rotational temperature $T_R \sim 10$ K, in good agreement with the gas temperature T_k deduced from CO measurements. This was an important result because (*a*) it extends the empirical correlation between T_R and T_k (see Figure 5) to the lower temperature regime; (*b*) as the NH_3 lines are less optically thick than the $J = 1$-0 line of CO, the good agreement between T_R and T_k confirms the absence of embedded heating sources; and (*c*) a confirmation of the low values of T_k supports earlier density estimates based on NH_3 measurements (e.g. Ho et al. 1977, Rydbeck et al. 1977). That the temperature is low in these regions means that very few of the rotational states will be populated. The two-level excitation model (Section 3.2) is then a good approximation, so that deduced densities $[n(H_2)]$ are reliable.

Extensive survey results of cloud conditions are now available (Ungerechts et al. 1982, Myers & Benson 1983). They indicate that $T_k \sim 10$ K and $n(H_2) \sim 10^4$–10^5 cm^{-3} are indeed typical values for the brightest NH_3 emission in dark clouds. In addition, mapping results indicate that the NH_3 emission delineates cold dense cores of typical size ~ 0.1 pc and typical mass $\sim 1\ M_\odot$. These dense cores, embedded in the more extended and diffuse CO envelopes (e.g. Martin & Barrett 1978, Snell 1981), may be the protostellar condensations that will form the next generation of stars (Silk 1980). From a spatial correlation study of dense cores against young

emission-line stars in the Taurus-Auriga region, Myers & Benson (1983) suggest that the numbers and time scales could indeed be consistent with the premise that the observed dense cores will form low-mass stars in the next few free-fall times ($\sim 10^6$ yr). In certain cases, large velocity motions observed in CO, as in L1551 (Snell et al. 1980) and TMC2 (Lichten 1982), infrared (Strom et al. 1976), and radio continuum emission, as in L1551 (Cohen et al. 1982), indicate that young stars have already formed within these condensations.

At present it is difficult to estimate the percentage of mass and volume of typical dark clouds that has condensed into dense cores. Complete surveys require improvements in sensitivity. Another important question is whether the dense cores are themselves centrally condensed. Higher angular resolution would be required to determine such detailed structures. With aperture synthesis, the spatial resolution at 100 pc will be better than $\sim 10^{15}$ cm, approaching the size of a solar nebula.

4.2 *Observations of Molecular Clouds: Clumping Effects*

The term *molecular cloud* usually refers to extended (10–100 pc) complexes associated with active OB star formation (cf. Blitz 1980, Evans 1981). Whereas most of these giant complexes are characterized by modest temperatures ($T_k \sim 10$ K) and densities [$n(H_2) \sim 10^2$ cm^{-3}], there are condensations with $T_k \sim 30$–100 K and $n(H_2) \sim 10^4$–10^6 cm^{-3} associated with compact H II regions, maser sources, and bright infrared objects. Early NH_3 observations (Morris et al. 1973) of large H II region complexes indicated rather weak intensities for the lower metastable transitions. Typical observed brightness temperatures are $T_a^*(NH_3) \sim 1$ K, compared with $T_a^*(CO) \sim T_k \sim 10$–50 K. With the detection of the satellite hyperfine structures (Mayer et al. 1973), it became clear that the NH_3 emission is moderately optically thick, with $\tau \sim 2$ for the main quadrupole hyperfine component. Since it would be very difficult to explain excitation temperatures for NH_3 inversion lines that were consistently below the kinetic temperature, these observations strongly indicated clumping of the molecular material into regions substantially smaller than the antenna beam width.

This line of argument is most convincing in the case of Kleinmann-Low (KL) nebula in the Orion molecular cloud (Barrett et al. 1977). Here a high gas temperature of $T_k \sim 70$–100 K and density of $n(H_2) \sim 10^5$ cm^{-3} are well established (cf. Turner et al. 1973, Linke & Goldsmith 1980, Gottlieb et al. 1975). With the inversion doublets thermalized, the observed values $\tau \sim 2$ and $T_B \sim 2$ K for the three lowest metastable lines imply that the NH_3 emission region must be considerably clumped with respect to the 1.5′ beam, with a size scale $\lesssim 15''$ (0.04 pc). Observations by Wilson et al.

(1979), Ziurys et al. (1981), and Batrla et al. (1981) with the 40″ Effelsberg beam agreed with this conclusion by finding correspondingly higher brightness temperature and a clumpier appearance than lower-resolution studies (see Figure 6).

Subsequent NH_3 observations of a variety of regions associated with active star formation (Schwartz et al. 1977, Little et al. 1980, Matsakis et al. 1980, Ho et al. 1981) support the conclusion that small-scale structures on the order of 0.05 pc are likely to be present. As more extensive mapping results became available (Ho et al. 1979, Little et al. 1980), it was further concluded that, based on the smoothness and extended nature of the NH_3 emission, there must be numerous clumps within the antenna beam and the clumping phenomenon itself must be extended. With the advent of the

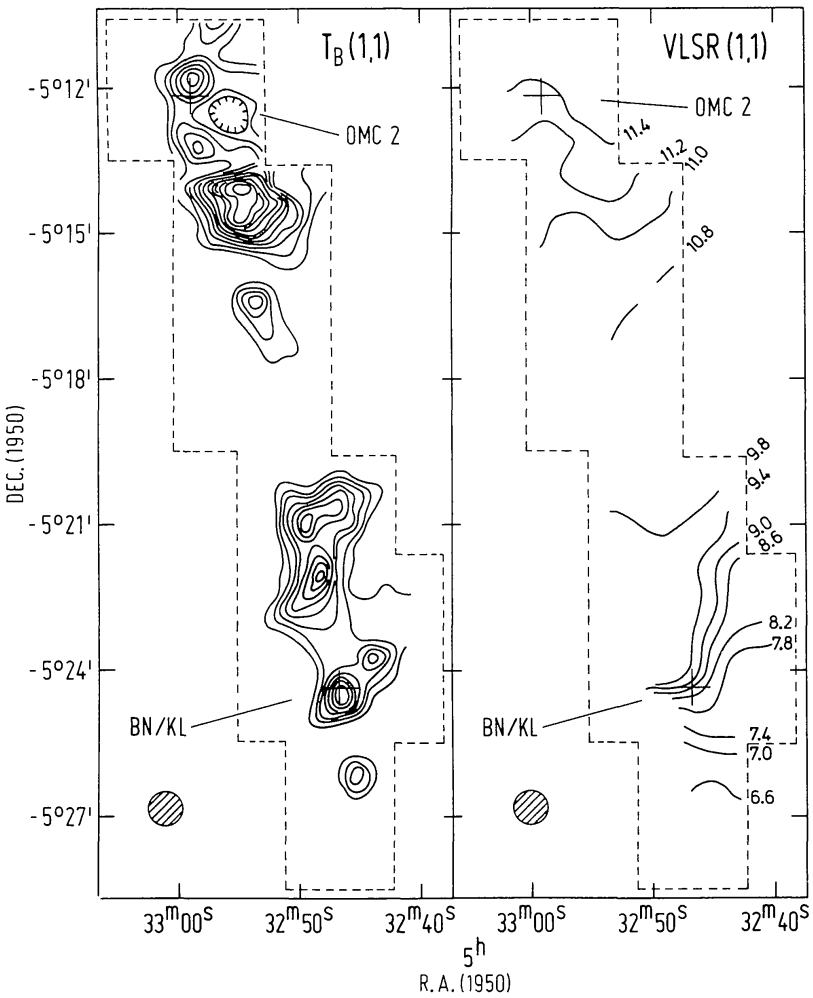

Figure 6 Fully sampled map of the Orion region in the $(J,K) = (1,1)$ line with 40″ angular resolution (Batrla et al. 1981). Complex structures are seen with a clumpy appearance.

VLA, both the KL region and the condensations $\sim 4'$ north of this region have now been studied with angular resolution ranging from 3–14″ (Genzel et al. 1982b, Pauls et al. 1983, Harris et al. 1983, Ho et al. 1983). Small-scale structures and interactions with young stars were found to have important effects on the observed emission profiles and spatial distributions (see Section 4.3).

Evidence of clumping has also been found in more distant regions: in DR 21 (Matsakis et al. 1977, 1981), where clumping allows unequal radiative trapping of the infrared transitions connecting the $(J, K) = (1, 1)$ and $(2, 1)$ states; in W3(OH) (Wilson et al. 1978, Ho & Barrett 1978a, Pauls & Wilson 1980), where the clumpy NH_3 emission apparently does not completely cover the background compact H II region; and in W51, where hot condensations have been observed directly with the VLA (see Section 4.3; Ho et al. 1983). Evidence for clumping has also been observed in H_2CO toward Orion and DR 21 (Evans et al. 1979, Dickel et al. 1983), where structures on the scale of 20″ can explain the excitation of H_2CO lines.

Clumpiness of molecular clouds is not surprising in itself. However, the deduced properties of the clumps may tell us much about cloud evolution and star formation. The most immediate implications concern mass and density estimates and their spatial distributions. Where clumping is important, the bulk of the mass appears to reside in small (~ 0.1 pc), dense ($\sim 10^5$ cm^{-3}) condensations. These properties are similar to those observed for the dense cores in nearby dark clouds (see Section 4.1), suggesting a common formation mechanism such as fragmentation. The difference is that in molecular clouds a large number of these condensations have been gathered into a relatively small volume. A second important implication of clumping is that beam-averaged properties observed with lower resolution, such as temperatures, motions, and gradients, may not represent the situation in real physical objects (see Section 4.3).

Not all parts of molecular clouds appear clumpy. There is an apparent dependence on how active the region is. Perhaps the best comparison is between Orion (Ho et al. 1979) and NGC 1333 (Ho & Barrett 1980). Both regions are at roughly the same distance, but the latter does not seem to be as active in forming young massive stars (only middle B stars; cf. Strom et al. 1974, Haschick et al. 1980). From excitation arguments, there also does not appear to be evidence of clumping in NGC 1333. Other regions with little or no clumping with respect to the antenna beam or the presence of many clumps, such as NGC 6334N (Schwartz et al. 1978) and dark clouds (Ungerechts et al. 1982, Myers & Benson 1983), are also devoid of massive OB stars. There is, therefore, a possible connection between the clumpiness of a region and the formation of massive stars.

4.3 *Hot Molecular Cores: Interferometric Observations*

With interferometry, condensations within molecular clouds are finally being resolved. Some of the oldest questions concerning positions relative to possible exciting sources, temperatures, masses, size scales, motion, and fraction of the total mass in condensations can be addressed observationally.

ORION The best-studied hot molecular condensation is the KL region in Orion. This region is quite complicated because of numerous kinematical components: an extended quiescent ($\Delta V \sim 3$ km s^{-1}) component, consisting of two features at 8.0 and 9.6 km s^{-1} that have overlapping spatial distributions (Ho & Barrett 1978b); a hot turbulent ($\Delta V \sim 10$ km s^{-1}) core at 4–5 km s^{-1} (Barrett et al. 1977, Wilson et al. 1979, Morris et al. 1980); and a possible "plateau" source ($\Delta V \sim 30$ km s^{-1}), which may either be related to the high-velocity CO emission (Wilson et al. 1979, Morris et al. 1980) or simply be the hyperfine satellite emission associated with the hot core (Genzel et al. 1982b). These kinematic features have different excitation conditions, as their relative contributions depend on the particular NH_3 transition. Because of the numerous infrared sources in the region (Downes et al. 1981) and the measured outflow of H_2O masers from the infrared source IRc2 (Genzel et al. 1981b), there is considerable interest in measuring the position of the hot thermal material in relation to the possible exciting sources. Single-dish measurements have been difficult (Morris et al. 1980, Zuckerman et al. 1981), while interferometric measurements have been more successful. At the time of this writing, aperture synthesis maps are available in 8 NH_3 transitions. Figure 7 shows high-resolution maps of the KL region in several NH_3 transitions (hot-core component) superposed on a 20-μm map (Ho et al. 1983b). There is good agreement between these maps. The NH_3 emission, $\sim$0.02 pc (10″) in extent, is displaced to the east of the infrared emission and tends to fill in the valleys between the peaks in the 20-μm map. Detailed comparisons of the maps allow several important conclusions to be drawn (Genzel et al. 1982b, Ho et al. 1983b): 1. The dominant effect is due to high column density. Optical depth of the NH_3 emission is high, with $\tau \sim 10$ for all observed transitions, so that apparent emission at high velocities can be explained in terms of satellite hyperfine emission. Pauls et al. (1983) argue that an additional high-velocity component is present with FWHM of 15–30 km s^{-1}, which may be related to the interaction of stellar winds with the hot ambient condensations. 2. Deduced H_2 column densities are high ($\sim 10^{24}$ cm^{-2}), so that extinction at 5–20 μm is $\sim$100 magnitudes at the NH_3 emission peaks. The anticorrelation between NH_3 emission and the 20-μm emission can be explained by extinction in the infrared by the NH_3-emitting region. 3. Brightness

temperatures are high, ~200 K at the peak. 4. Emission structure in the optically thick main quadrupole hyperfine component appears similar to that of the optically thin satellite hyperfine component in the (4, 4) line. Hence emission peaks correspond to excitation peaks as well as column-density peaks. 5. There is some indication that excitation increases toward IRc2. 6. Observed motion is turbulent, with some evidence for expansion. 7. The hot-core emission observed with the VLA essentially accounts for all of the single-dish emission for this kinematic component. The mass involved is on the order of 1 $M_\odot$. 8. The emission over different velocities exhibits clumpiness. 9. Lower-brightness emission of the quiescent component (see above) may be missed on the VLA because of present receiver sensitivity.

Aperture synthesis maps (Harris et al. 1983) in the (1, 1) and (2, 2) inversion lines have also been made for the condensation 4′ north of the KL region (Batrla et al. 1981). Two small fragments, ~0.05 pc (20″) in size, are resolved with 14″ resolution (see Figure 8). These observations are

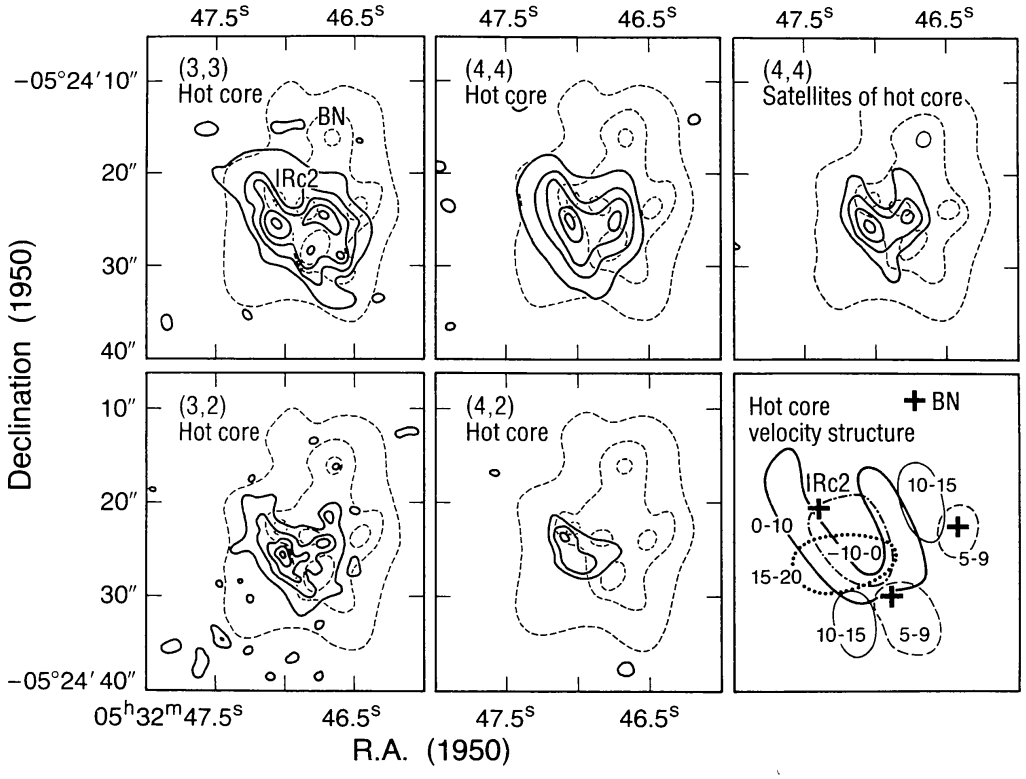

Figure 7 VLA maps of the hot-core component of the Orion-KL region with 2.7″ angular resolution (Ho et al. 1983b). The dashed contours are the 20-μm distribution. Note the similarity of the emission both in the main and satellite hyperfine components. This similarity suggests that observed peaks are maxima in excitation, both in temperature and density. The emission is seen to be more closely associated with IRc2, especially for the (4, 2) transition, which has the highest excitation of all the transitions shown. There is some systematic trend in the emission velocity, e.g. the highest and lowest velocities appear well centered.

important for their contrast with the KL region. Here the peak brightness temperatures are only ~ 20 K. The optical depth of the main quadrupole hyperfine is ~ 7 for the (1, 1) line and ~ 3 for the (2, 2) line. The mass is estimated to be on the order of 1–10 $M_\odot$. The two fragments are further observed to be rotating at ~ 30 km s^{-1} pc^{-1}, which is large enough for stabilization against gravitational collapse. By comparison with single-dish intensities, it is estimated that only $\sim 10\%$ of the emission resides in the two fragments. The rest of the emission arises from an extended component with lower optical depth. The greater spatial extent, the lower temperatures, the lower optical depth, and the dominance of systematic motion as opposed to turbulence all suggest an evolutionary state earlier than that of the KL region. The large velocity gradient is especially interesting, for it suggests that these fragments have not yet succeeded in getting rid of their angular momentum.

W51 VLA maps in the (3, 3) inversion line with 1.8–2.5″ angular resolutions have been made for this distant H II region complex (Ho et al. 1983a). Three small (~ 0.1 pc), warm (~ 100 K) NH_3 condensations were found associated with the most compact H II regions in W51 (see Figure 9). The warm molecular cores were found to be displaced slightly with respect to the H II regions but very well centered with H_2O and OH masers in the region. Because of the warm temperatures, it is likely that the NH_3 emission region is dense ($\sim 10^5$ cm^{-3}). The observed small size is larger than that observed for the condensation in Orion. This may indicate further substructures. The better spatial correlation of the hot molecular material with the maser sources known to have large proper motions (Genzel et al. 1981a, Schneps et al. 1981) suggests that localized heating may be produced by interactions with outflowing material from young stars. The displacement from the nearby compact H II region also suggests that these molecular conden-

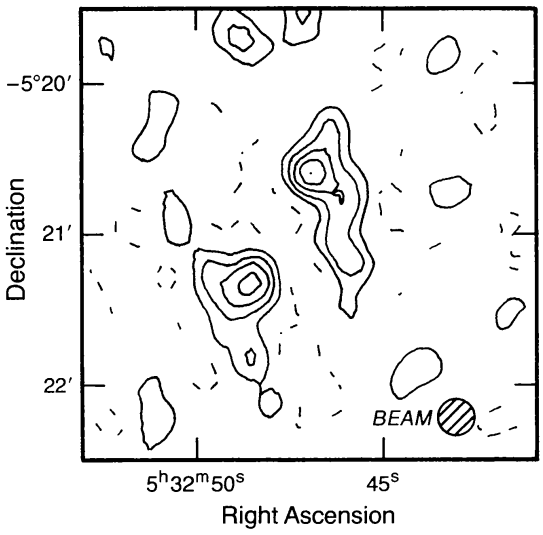

Figure 8 VLA map of the condensations 4′ north of the Orion-KL region (Harris et al. 1983). The $(J, K) = (1, 1)$ emission shows that these condensations are in fact rotating at ~ 30 km s^{-1} pc^{-1}, which is sufficient to stabilize against collapse.

sations may be associated with embedded sources not yet detectable with radio continuum. Indeed, the condensation associated with W51IRS2 appears to be excited by a separate 8-μm source IRS2-East (Genzel et al. 1982a). The warm NH_3 emission also represents considerable extinction. As in the case of Orion (Genzel et al. 1982b), heavy extinction may obscure

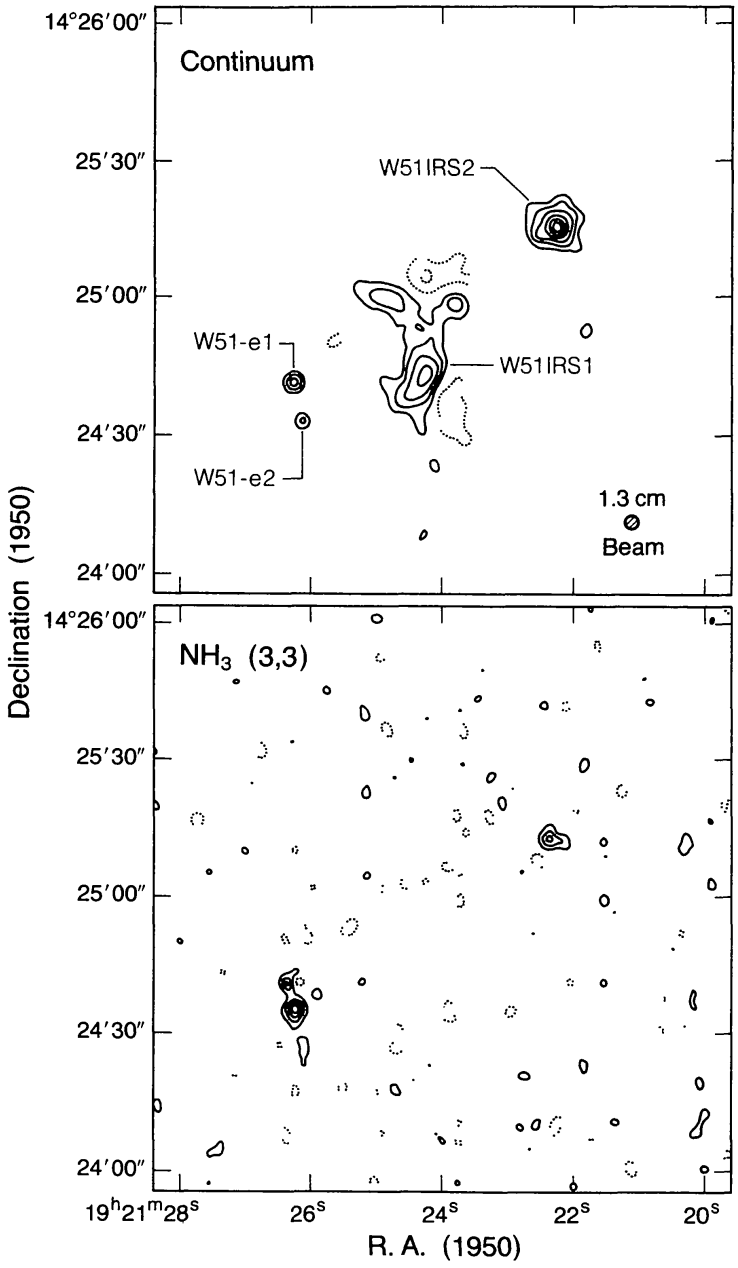

Figure 9 (*top*) 1.3-cm continuum map of the W51 region. (*bottom*) NH_3 map of the same region in the $(J, K) = (3, 3)$ line (Ho et al. 1983a). The observed NH_3 condensations are warm ($\sim$100 K) and are offset from the compact H II regions. The molecular condensations correlate very well with H_2O and OH masers, suggesting interactions (heating) with an outflow or embedded, undetected exciting stars.

embedded exciting sources even at mid-infrared wavelengths. The detection of compact regions of heated gas may be the best means to locate the very young objects.

SAGITTARIUS A The properties of the Galactic center region have been reviewed by Oort (1977). The molecular material is dominated by two giant molecular clouds: Sagittarius A (Sgr A) on the negative longitude side and Sagittarius B2 (Sgr B2) on the positive longitude side. These molecular complexes are of great interest because they are very close to the Galactic center, within ~ 300 pc, and are characterized by unusually large internal motions with observed line widths of 20–100 km s^{-1}. The emission in various molecules has been surveyed (cf. Fukui et al. 1977, 1980, Liszt et al. 1977). In NH_3, surveys along the plane were made with 5'.3 resolution (Kaifu et al. 1975) and 40″ resolution (Gusten et al. 1981). Figure 10 shows the $(J, K) = (1, 1)$ emission of the Sgr A complex within $\sim 0.2°$ of the nucleus. The condensations at various velocities have been confirmed by $(J, K) = (3, 3)$ observations with 1'.5 resolution (Armstrong 1983).

By comparing the intensities of the (1, 1), (2, 2), and (4, 4) transitions, Gusten et al. (1981) concluded that the gas temperature is in the range 50–120 K over the entire Sgr A complex. Further NH_3 observations of higher rotational levels (Walmsley, 1983, private communication) support this interpretation. These are important conclusions, since infrared observations at 30–100 μm (Gatley et al. 1977), 540 μm (Hildebrand et al. 1978),

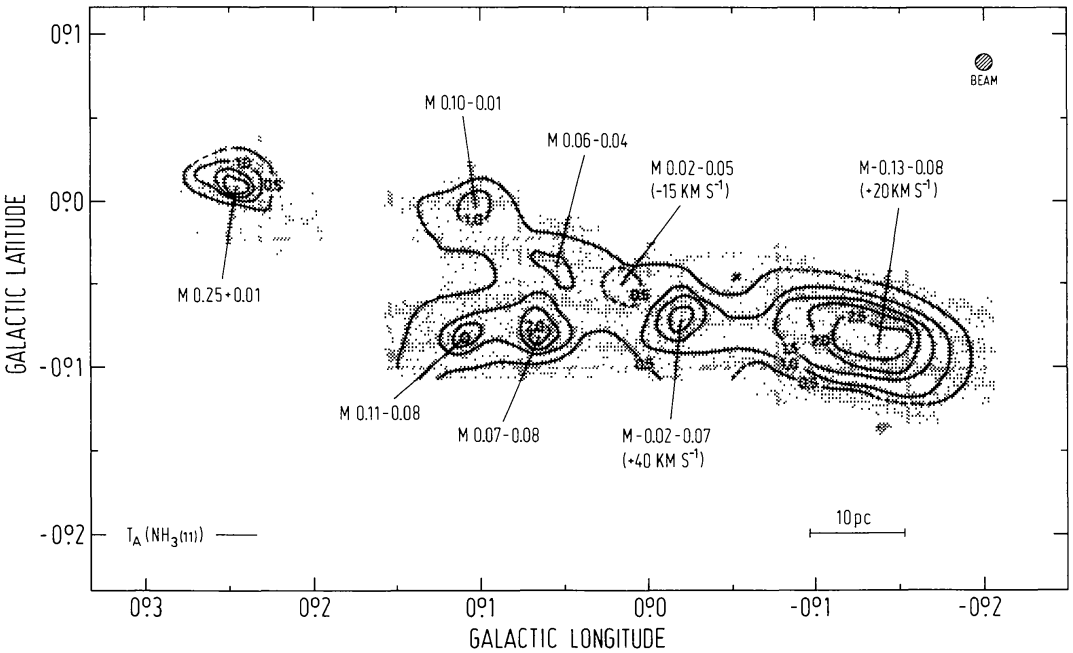

Figure 10 $(J, K) = (1, 1)$ NH_3 emission near the Galactic center (Gusten et al. 1981). Numerous condensations are seen.

and 40–250 μm (Odenwald 1982) indicate dust color temperatures less than 40 K. If the gas temperature is indeed hotter than the ambient dust, a direct heating mechanism such as cosmic rays (with an ionization rate $\sim 10^2$ times the Galactic value) may be required, as suggested by Gusten et al. (1981). Some alternatives remain. Cold, optically thick foreground dust can obscure warmer embedded dust. This may be suggested by the poor spatial correlation between 540-μm emission and the 40–250 μm emission (Odenwald 1982). Embedded heating sources may be present, although undetected so far. Existing continuum studies (cf. Downes et al 1978) are limited in sensitivity to spectral types earlier than B0. Certainly by comparison to Sgr B2, the Sgr A complex appears to be in an earlier evolutionary state, with less apparent active star formation. Gusten & Downes (1980) have suggested that Sgr A lies closer (~ 100 pc) to the Galactic center than Sgr B2 (~ 300 pc). The excitation mechanism of the molecular material remains unclear at present, although the solution of this problem may have important implications for the evolution of the nucleus itself.

The VLA observations of M-0.13-0.08 (Amstrong et al. 1983) indicate that only $\sim 15\%$ of the emission observed in single-dish studies arises in several clumps with intrinsic size scales on the order of ~ 1 pc ($\sim 20''$). These clumps have brightness temperatures of ~ 30 K, line widths of ~ 5–10 km s^{-1}, and exhibit a velocity gradient of ~ 6 km s^{-1} pc^{-1}. These results suggest the following: 1. The bulk of the emission is extended ($\gtrsim 1'$) with brightness $\lesssim 20$ K. 2. The velocity gradient in the inner 2–3 pc of M-0.13-0.08 observed with 5–10″ resolution is about a factor of 3 greater than that in the outer 10 pc observed with 40″ resolution. 3. The presence of a number of clumps may complicate the analysis of lower-resolution data in that emission in different transitions may arise from different spatial volumes. Hence, averages over the beam may not be representative of any of the components. 4. The condensations observed in Sgr A are massive ($\gtrsim 10^3$ $M_\odot$ each), in contrast with the value of 1–10 $M_\odot$ for the dense cores in Orion. The aggregation of clumpy material, although similar to other molecular clouds, may be on a more massive scale in Sgr A. 5. The kinematics in the region is complicated. Superposed on the velocity gradient along the plane are motions that may reflect large-scale turbulence. Are such motions related to the gravitational fields or activity peculiar to the nucleus?

The interferometric studies have demonstrated that molecular clouds are indeed clumpy. In particular, numerous condensations are found to be closely associated with young massive stars. In general, only a small fraction by mass ($\sim 10\%$) of the complexes appears to have condensed. In more quiescent regions, the typical size scale is ~ 0.1 pc and the typical mass

is $\sim$1–10 $M_\odot$. In more active regions associated with more massive stars, condensations appear both larger and more massive.

4.4 *Extragalactic Ammonia*

With the good sensitivity of the 100-m Effelsberg telescope, NH_3 was successfully detected in the spiral galaxies IC 342 (4.5 Mpc) and NGC 253 (3.4 Mpc) via the $(J, K) = (1, 1)$ inversion line (Martin & Ho 1979). This was followed by the detection of the (2, 2) line in IC 342 (Martin et al. 1982). The observed spectra are shown in Figure 11. These emission lines were excruciatingly weak, but their detection meant that gas temperatures in external galaxies can be directly measured for the first time. Although optically thick CO can be detected much more easily in external galaxies (Rickard 1979, Morris & Rickard 1982), gas temperatures cannot be deduced because of the uncertain role of severe beam dilution. With the NH_3 lines the temperature measurement derives from the ratio of line strengths (see Section 3.2). Since the NH_3 optical depths are, in general, modest and the excitations of the two lines are comparable, the beam dilution effects are canceled out in taking a ratio.

The nearly equal intensity of the (1, 1) and (2, 2) lines in IC 342 implies the existence of warm (50 ± 20 K) gas (see Figures 4 and 5). The intensity of the emission then sets a lower limit of 25 pc to the equivalent size of the emission complex. Consideration of the different alternatives led to

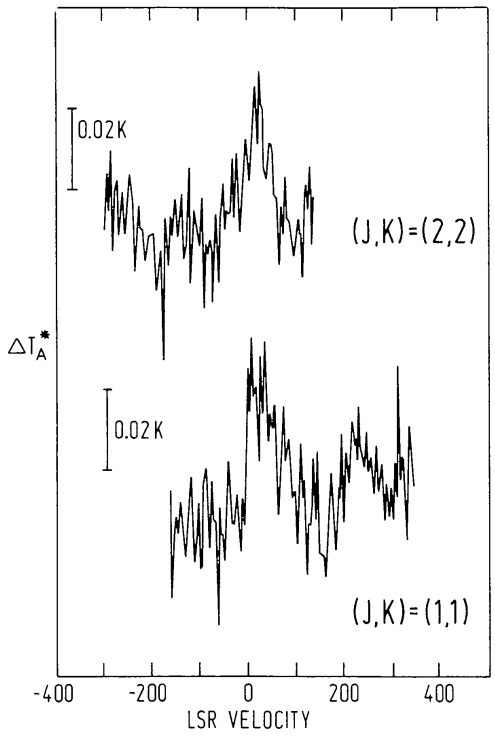

Figure 11 The observed NH_3 spectra toward the spiral galaxy IC 342 (Ho et al. 1982). The observed velocity and line width are in good agreement with CO and H I observations.

the conclusion that gas-dust collisions may be the likeliest heating mechanism (Ho et al. 1982). For collisions to be effective, densities must be high ($\gtrsim 10^5$ cm^{-3}). From excitation arguments, this then implies an upper limit of 30 pc to the scale size. Finally, by comparing the results with the observed properties of molecular complexes in the Galaxy, it was concluded that the likeliest configuration for the NH_3 emission region in IC 342 is a highly fragmented one. A plausible model consists of a conglomeration of 10^2–10^4 hot molecular cores, each with an embedded OB cluster. This appears to be consistent with CO and radio continuum observations. Since Becklin et al. (1980) have detected extended 10-μm emission, and Turner & Ho (1983) have detected extended thermal radio continuum emission, both on the scale of $\sim$200 pc, it is likely that the NH_3 emission is also extended on this scale.

To determine the spatial extent of the NH_3 emission, Ho & Martin (1983) made aperture synthesis maps with the VLA. NH_3 was not detected, establishing a 3σ upper limit of 0.5 K in brightness temperature referred to a 6″ beam. A comparison of the brightness temperatures shows that less than 30% of the detected flux with the 40″ beam of the Effelsberg telescope can be localized in any one 6″ area synthesized with the VLA. The implication is that the NH_3 emission must be distributed on a scale larger than 130 pc.

These preliminary results on extragalactic NH_3 demonstrate its usefulness in studying molecular material in the external galaxies. With improved sensitivity at Effelsberg and the VLA, we can begin to address such questions as the distribution of molecular material in the spiral arms as compared with the nucleus, the relation of neutral matter to star formation in the nuclei of galaxies, and the dynamics of the molecular material.

4.5 *Far-Infrared and Submillimeter Observations of Ammonia*

With improvements in detector technology and Fabry-Perot techniques (Storey et al. 1980), the rotation-inversion transition $(J, K) = (4, 3)^a \rightarrow (3, 3)^s$ of NH_3 at 125 μm has been detected in emission toward the KL region (Figure 12; Townes et al. 1983). These measurements have been difficult because of atmospheric extinction at sea level and interfering telluric absorption lines even at the high altitude attained by the NASA Kuiper Airborne Observatory. Furthermore, high-density gas is required to produce frequent enough excitation to the upper rotational level; this high density (e.g. $n > 10^7$ cm^{-3}) usually occurs in only a small solid angle, and is accompanied by dust, which can be expected to be optically thick even at 100 μm. The $(4, 3)^a \rightarrow (3, 3)^s$ line observed was in emission, and so required collisional rather than far-infrared excitation. Furthermore, it was much broader than the inversion transitions seen in this region, indicating a large

optical depth so that small amounts of high-velocity gas were detected. At microwave frequencies, both the (4, 3) and (3, 3) inversion doublets have been detected toward the KL region, and from this the optical depth of the far-infrared transitions may be estimated. Since the hot-core component (Section 4.3) is the only region dense enough to provide the observed rate

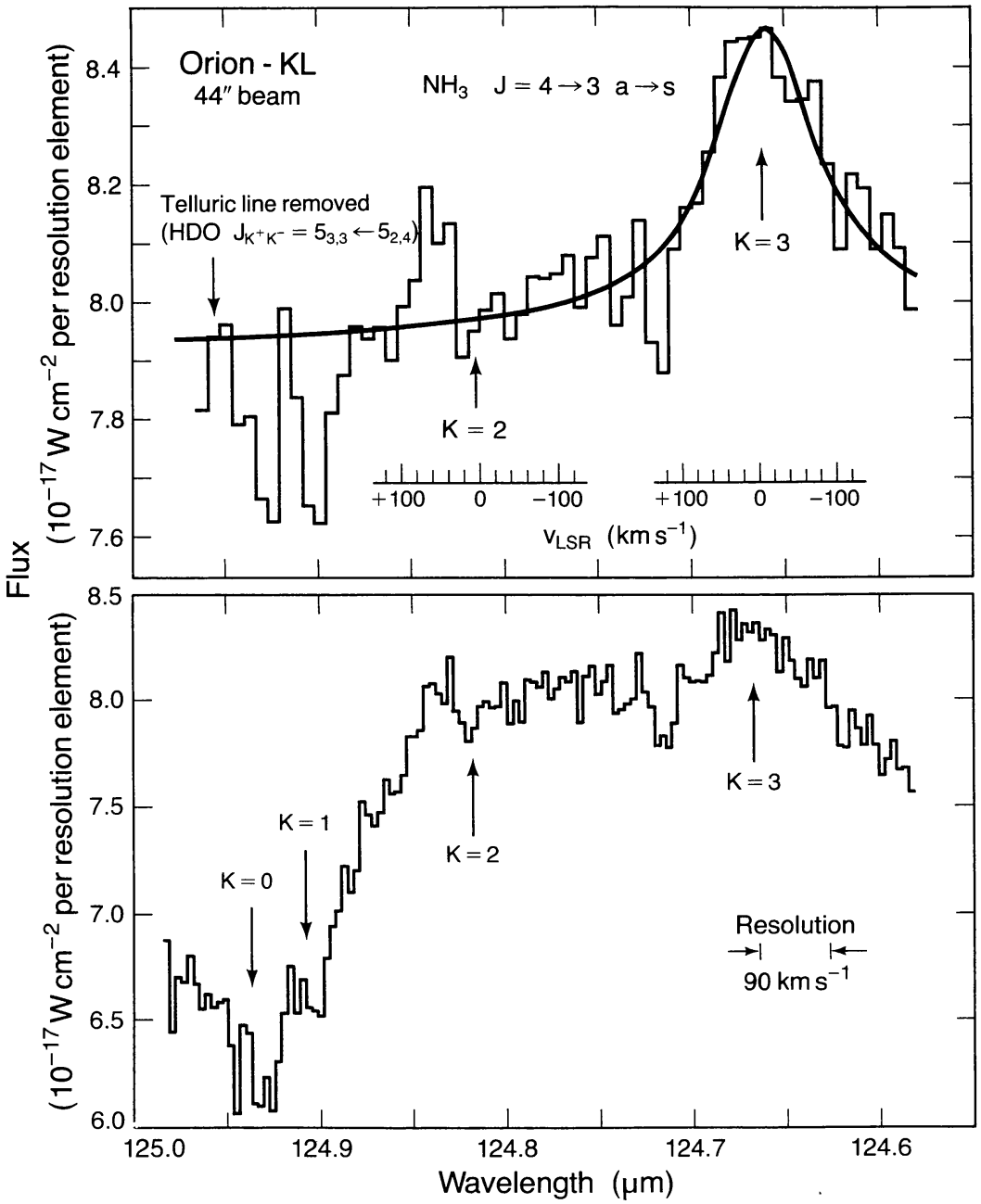

Figure 12 The $(4,3)^a \rightarrow (3,3)^s$ far-infrared line at 125 μm detected toward the Orion-KL region before (*bottom*) and after (*top*) the removal of a telluric absorption line (Townes et al. 1983). The line has a line width of ~ 50 km s^{-1} after deconvolution of instrumental profile, a brightness temperature of ~ 30 K, and a suspected optical depth of ~ 300.

of collisionally excited photons, Townes et al. (1983) argue that this component dominates at far-infrared wavelengths. They estimate, for the $(4,3)^a \rightarrow (3,3)^s$ line, that $\tau \sim 300$. For such high opacities, radiative transfer must be treated carefully. For straightforward collisional excitation (Section 3.2), where radiative trapping essentially lengthens the radiative lifetime by τ, excitation of the far-infrared NH_3 line requires a density of $\sim 10^7$ cm^{-3}. This is consistent with estimates based on the radio lines. Since the line is seen in emission, the gas must be hotter than the opaque dust.

Using a bolometer heterodyne receiver and the Kuiper Airborne Observatory, Keene et al. (1983) have now detected the $(1,0) \rightarrow (0,0)$ ground rotational transition at 524 μm (572 GHz). Because of nuclear spin statistics, the $K = 0$ ladder does not have inversion lines (see Section 1.1). Hence the (0, 0) ground state can be studied only by infrared transitions. The observed emission appears localized to the KL region (Figure 13). The observed line profile (Figure 13*a*) peaks at 9 km s^{-1}, indicating that the bulk

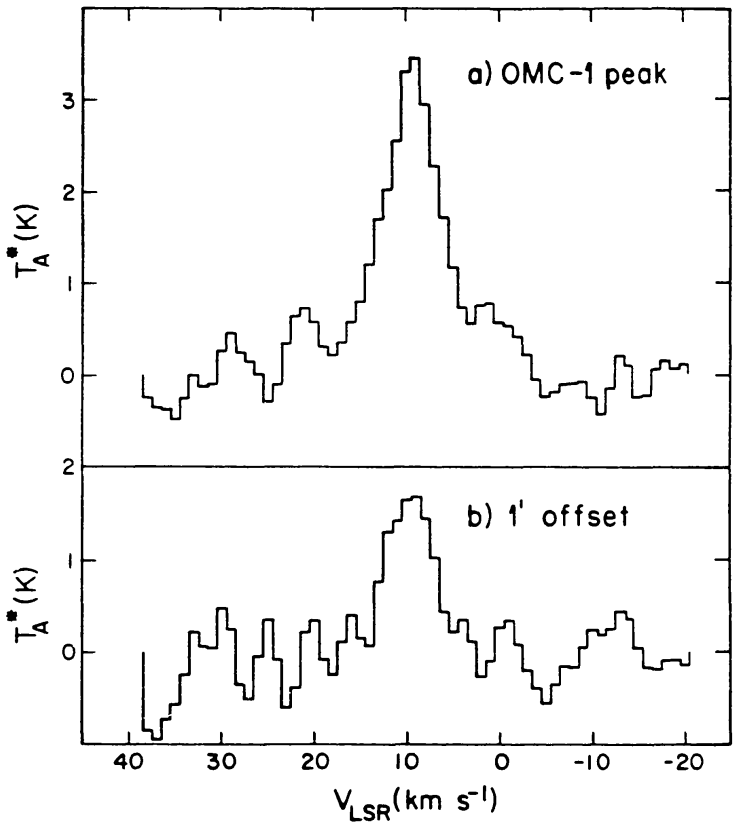

Figure 13 The $(1,0) \rightarrow (0,0)$ submillimeter line at 524 μm observed (*a*) toward Orion-KL and (*b*) at 1′ offset positions. The data were taken on board of the Kuiper Airborne Observatory by Keene et al. (1983). The line is probably optically thick, and arises from the quiescent cloud component rather than the hot core.

of the emission arises from the quiescent molecular material rather than the hot-core component. The observed brightness temperature of this line is 3.5 K. This could be due to either subthermal excitation because of the large value of Einstein A (Table 1), or a small beam-filling factor. Estimated column densities suggest that this transition is optically quite thick.

4.6 *Mid-Infrared Observations of Ammonia*

Infrared heterodyne spectroscopy of NH_3 in stars was recently reviewed by Betz (1981). The first heterodyne detection of the NH_3 vibration-rotation lines, in the 10-μm atmospheric window, was reported by Betz et al. (1979). These transitions are especially valuable because they allow us to sample the ground state $(J, K) = (0, 0)$ level, which does not have inversion lines in the radio wavelengths; furthermore, the rotational transition to this level falls in the far-infrared, where the atmosphere is opaque (see Section 4.5). At the mid-infrared, diffraction-limited optical telescopes provide angular resolutions of $\sim 1''$ (~ 1000 AU at 1 Kpc), which allow one to resolve and study circumstellar envelopes of late-type stars in detail. By observing several ν_2 vibration-rotation lines near 10.5 μm arising from states of various excitation energies (Figure 14) toward IRC+10216, one can study the acceleration of hotter material, sampled by the $aQ(3, 2)$ transition, relative to the cooler material, sampled by the $aR(0, 0)$ transition. Furthermore, good relative intensities or upper limits have been obtained for the higher excitation transitions. Betz (1981) concludes that most of the circumstellar NH_3 in this source is at temperatures of $\lesssim 700$ K. These results also give a mass outflow of $\sim 5 \times 10^{-4}\ M_\odot\ \mathrm{yr}^{-1}$ from the central arcsec of the circumstellar material (Betz et al. 1979).

Successful vibration-rotation line observations have also been made toward the OH/IR supergiants VY CMa, VXSgr, and IRC+10420 (McLaren & Betz 1980). These detections are particularly interesting because NH_3 absorptions were detected at velocities coincident with OH maser features. Since the NH_3 absorption occurs along the line of sight to the star, absolute positions (to $\sim 0.2''$) can thereby be obtained for specific maser spots.

5. PROSPECTUS

The study of interstellar NH_3 is at an exciting juncture. With the successful application of interferometry at radio wavelengths, and Fabry-Perot and heterodyne techniques in the infrared, very-small-scale structures and highly excited regions of the interstellar medium can be studied. With the anticipated improvements in receiver sensitivity at the VLA and at the

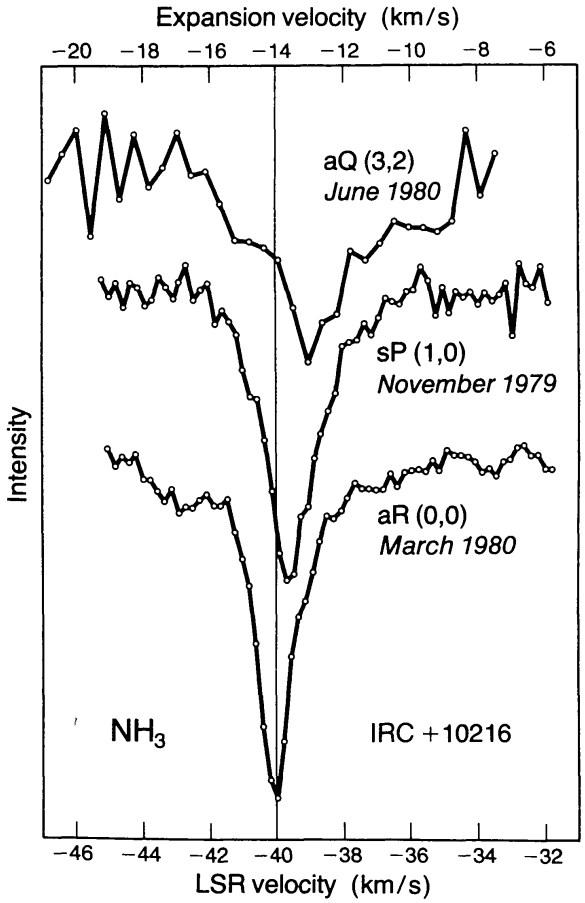

Figure 14 The 10-μm vibration-rotation lines observed toward IRC+10216 (Betz 1981). Note the velocity differences with excitation energy. The higher-excitation $aQ(3, 2)$ line appears to be from material still under acceleration, whereas the lower-excitation $aR(0, 0)$ line may correspond to that part of the circumstellar shell that has already reached terminal velocity. The vertical scales of the $aQ(3, 2)$ and $sP(1, 0)$ lines have been multiplied by a factor of 5 and 1.5, respectively.

Effelsberg telescope, the range of phenomena and the accessible NH_3 universe will be greatly expanded at $\lambda \sim 1$ cm. Similarly, improvements in sensitivity and resolution will greatly increase the ability to study very hot and dense regions, such as interstellar shocks and circumstellar envelopes. Finally, the prospect of studying extragalactic molecular material at 1″ resolution is most exciting indeed.

ACKNOWLEDGMENTS

We thank our colleagues who have collaborated with us over the years, and the many colleagues who have shared their results in advance of publication.

Literature Cited

Armstrong, J. T. 1983. PhD thesis. Mass. Inst. Technol.

Armstrong, J. T., Ho, P. T. P., Barrett, A. H. 1983. *Ap. J. Lett.* Submitted for publication

Barrett, A. H., Ho, P. T. P., Myers, P. C. 1977. *Ap. J. Lett.* 211:L39

Batchelor, R. A., Gardner, F. F., Knowles, S. H., Mebold, U. 1977. *Proc. Astron. Soc. Aust.* 3:152

Batrla, W., Bastien, P., Wilson, T. L., Ruf, K., Pauls, T., Martin, R. N. 1981. *Mitt. Astron. Ges.* 54:278

Becklin, E. E., Gatley, I., Matthews, K., Neugebauer, G., Sellgren, K., Werner, M. W., Wynn-Williams, C. G. 1980. *Ap. J.* 236:441

Betz, A. L. 1981. In *Laser Spectroscopy V*, ed. A. R. W. McKellar, T. Oka, B. P. Stoicheff, p. 81. Springer-Verlag

Betz, A. L., McLaren, R. A., Spears, D. L. 1979. *Ap. J. Lett.* 229:L97

Betz, A. L., McLaren, R. A., Sutton, E. C., Johnson, M. A. 1977. *Icarus* 30:650

Blitz, L. 1980. In *Giant Molecular Clouds in the Galaxy*, ed. P. M. Solomon, M. G. Edmonds, p. 1. Oxford: Pergamon

Cheung, A. C., Chui, M. F., Matsakis, D., Townes, C. H., Yngvesson, K. S. 1973. *Ap. J. Lett.* 186:L73

Cheung, A. C., Rank, D. M., Townes, C. H., Knowles, S. H., Sullivan, W. T. III. 1969. *Ap. J. Lett.* 157:L13

Cheung, A. C., Rank, D. M., Townes, C. H., Thornton, D. D., Welch, W. J. 1968. *Phys. Rev. Lett.* 21:1701

Cohen, M., Bieging, J. H., Schwartz, P. R. 1982. *Ap. J.* 253:707

Dalgarno, A. 1982. In *Applied Atomic Collision Physics*, 1:427. Academic

Dickel, H. R., Lubenow, A. F., Goss, W. M., Forster, J. R., Rots, A. H. 1983. *Astron. Astrophys.* In press

Dickinson, D. F., Gulkis, S., Klein, M. J., Kuiper, T. B. H., Batty, M., et al. 1982. *Astron. J.* 87:1202

Downes, D., Genzel, R., Becklin, E. E., Wynn-Williams, C. G. 1981. *Ap. J.* 244:869

Downes, D., Goss, W. M., Schwarz, V. J., Wouterloot, J. G. A. 1978. *Astron. Astrophys. Suppl.* 35:1

Evans, N. J. II. 1981. In *Infrared Astronomy, IAU Symp. No. 96*, ed. C. G. Wynn-Williams, D. P. Cruikshank, p. 107. Dordrecht: Reidel

Evans, N. J. II, Plambeck, R. L., Davis, J. H. 1979. *Ap. J. Lett.* 227:L25

Fehsenfeld, F. C., Lindenger, W., Schmeltekopf, A. L., Albritton, D. L., Ferguson, E. E. 1975. *J. Chem. Phys.* 62:2001

Fukui, Y., Iguchi, T., Kaifu, N., Chikada, Y. 1977. *Publ. Astron. Soc. Jpn.* 29:643

Fukui, Y., Kaifu, N., Morimoto, M., Miyaji, T. 1980. *Ap. J.* 241:147

Gatley, I., Becklin, E. E., Werner, M. W., Wynn-Williams, C. G. 1977. *Ap. J.* 216:277

Genzel, R., Becklin, E. E., Wynn-Williams, C. G., Moran, J. M., Reid, M. J., et al. 1982a. *Ap. J.* 255:527

Genzel, R., Downes, D., Ho, P. T. P., Bieging, J. 1982b. *Ap. J. Lett.* 259:L103

Genzel, R., Downes, D., Schneps, M. H., Reid, M. J., Moran, J. M., et al. 1981a. *Ap. J.* 247:1039

Genzel, R., Reid, M. J., Moran, J. M., Downes, D. 1981b. *Ap. J.* 244:884

Gottlieb, C. A., Lada, C. J., Gottlieb, E. W., Lilley, A. E., Litvak, M. M. 1975. *Ap. J.* 202:655

Green, S. 1980. *J. Chem. Phys.* 73:2740

Green, S. 1982. *NASA Tech. Memo. 83869*

Greenberg, L., McLaren, R., Stoller, L., Townes, C. H. 1977. *Proc. Symp. Recent Results Infrared Astrophys.*, ed. P. Dyal, p. 9. *NASA Tech. Memo. X-73190*

Gusten, R., Downes, D. 1980. *Astron. Astrophys.* 87:6

Gusten, R., Walmsley, C. M., Pauls, T. 1981. *Astron. Astrophys.* 103:197

Harris, A., Townes, C. H., Matsakis, D. N., Palmer, P. 1983. *Ap. J. Lett.* 265:L63

Haschick, A. D., Moran, J. M., Rodriguez, L. F., Burke, B. F., Greenfield, P., Garcia-Barreto, J. A. 1980. *Ap. J.* 237:26

Herbst, E., Klemperer, W. 1973. *Ap. J.* 185:505

Hildebrand, R. H., Whitecomb, S. E., Winston, R., Stiening, R. F., Harper, D. A., Moseley, S. H. 1978. *Ap. J. Lett.* 219:L101

Ho, P. T. P., Barrett, A. H. 1978a. *MNRAS* 184:93p

Ho, P. T. P., Barrett, A. H. 1978b. *Ap. J. Lett.* 224:L23

Ho, P. T. P., Barrett, A. H. 1980. *Ap. J.* 237:38

Ho, P. T. P., Barrett, A. H., Myers, P. C., Matsakis, D. N., Cheung, A. C., et al. 1979. *Ap. J.* 234:912

Ho, P. T. P., Genzel, R., Das, A. 1983a. *Ap. J.* 266:596

Ho, P. T. P., Genzel, R., Downes, D. 1983b. Preprint

Ho, P. T. P., Martin, R. N. 1983. *Ap. J.* In press

Ho, P. T. P., Martin, R. N., Barrett, A. H. 1978. *Ap. J. Lett.* 221:L117

Ho, P. T. P., Martin, R. N., Barrett, A. H. 1981. *Ap. J.* 246:761

Ho, P. T. P., Martin, R. N., Myers, P. C., Barrett, A. H. 1977. *Ap. J. Lett.* 215:L29

Ho, P. T. P., Martin, R. N., Ruf, K. 1982. *Astron. Astrophys.* 113:155
Kaifu, N., Morris, M., Palmer, P., Zuckerman, B. 1975. *Ap. J.* 201:98
Keene, J., Blake, G. A., Phillips, T. G. 1983. *Ap. J. Lett.* In press
Knacke, R. F., McCorkle, S., Puetter, R. C., Erickson, E. F., Kratschmer, W. 1982. *Ap. J.* 260:141
Kukolich, S. G. 1967. *Phys. Rev.* 156:83
Kwok, S., Bell, M. B., Feldman, P. A. 1981. *Ap. J.* 247:125
Lang, K. R., Willson, R. F. 1980. *Ap. J.* 238:867
Lichten, S. M. 1982. *Ap. J. Lett.* 255:L119
Linke, R. A., Goldsmith, P. F. 1980. *Ap. J.* 235:437
Liszt, H. S., Burton, W. B., Sanders, R. H., Scoville, N. Z. 1977. *Ap. J.* 213:38
Little, L. T., Brown, A. T., Macdonald, G. H., Riley, P. W., Matheson, D. N. 1980. *MNRAS* 193:115
Little, L. T., Matheson, D. N., Riley, P. W. 1977. *MNRAS* 181:33p
Macdonald, G. H., Little, L. T., Brown, A. T., Riley, P. W., Matheson, D. N., Felli, M. 1981. *MNRAS* 195:387
Martin, R. N., Barrett, A. H. 1978. *Ap. J. Suppl.* 36:1
Martin, R. N., Ho, P. T. P. 1979. *Astron. Astrophys.* 74:L7
Martin, R. N., Ho, P. T. P., Ruf, K. 1982. *Nature* 296:632
Matsakis, D. N., Bologna, J. M., Schwartz, P. R., Cheung, A. C., Townes, C. H. 1980. *Ap. J.* 241:655
Matsakis, D. N., Brandshaft, D., Chui, M. F., Cheung, A. C., Yngvesson, K. S., et al. 1977. *Ap. J. Lett.* 214:L67
Matsakis, D. N., Hjalmarson, Å, Palmer, P., Cheung, A. C., Townes, C. H. 1981. *Ap. J. Lett.* 250:L85
Mayer, C. H., Waak, J. A., Cheung, A. C., Chui, M. F. 1973. *Ap. J. Lett.* 182:L65
McLaren, R. A., Betz, A. L. 1980. *Ap. J. Lett.* 240:L159
Mitchell, G. F., Ginsburg, J. L., Kuntz, P. J. 1978. *Ap. J. Suppl.* 38:39
Moore, C. R., Clauss, R. C. 1979. *IEEE Trans. Microwave Theory Tech.* 27:249
Morris, M., Palmer, P., Zuckerman, B. 1980. *Ap. J.* 237:1
Morris, M., Rickard, L. J 1982. *Ann. Rev. Astron. Astrophys.* 20:517
Morris, M., Zuckerman, B., Palmer, P., Turner, B. E. 1973. *Ap. J.* 186:501
Myers, P. C., Benson, P. J. 1980. *Ap. J. Lett.* 242:L87
Myers, P. C., Benson, P. J. 1983. *Ap. J.* 266:309
Odenwald, S. F. 1982. PhD thesis. Harvard Univ.
Oka, T. 1968a. *J. Chem. Phys.* 48:4919
Oka, T. 1968b. *J. Chem. Phys.* 49:3135
Oka, T., Shimizu, F. O., Shimizu, T., Watson, J. K. G. 1971. *Ap. J. Lett.* 165:L15
Oort, J. H. 1977. *Ann. Rev. Astron. Astrophys.* 15:295
Pauls, T., Wilson, T. L. 1980. *Astron. Astrophys.* 91:L11
Pauls, T. A., Wilson, T. L., Bieging, J. H., Martin, R. N. 1983. *Astron. Astrophys.* Submitted for publication
Phillips, T. G., Jefferts, K. B. 1974. *IEEE Trans. Microwave Theory Tech.* 22:1290
Plambeck, R. L., Wright, M. C. H., Welch, W. J., Bieging, J. H., Baud, B., et al. 1982. *Ap. J.* 259:617
Prasad, S. S., Huntress, W. T. Jr. 1980. *Ap. J.* 239:151
Rickard, L. J 1979. In *The Large Scale Characteristics of the Galaxy, IAU Symp. No. 84*, ed. W. B. Burton, p. 413. Dordrecht: Reidel
Rydbeck, O. E. H., Sume, A., Hjalmarson, A., Ellder, J., Ronnang, B. O., Kollberg, E. 1977. *Ap. J. Lett.* 215:L35
Scalise, E. Jr., Schaal, R. E., Bakov, Y., Vilas Boas, J. W. S., Myers, P. C. 1981. *Astron. J.* 86:1939
Schneps, M. E., Lane, A. P., Downes, D., Moran, J. M., Genzel, R., Reid, M. J. 1981. *Ap. J.* 249:124
Schwab, F. 1980. *Proc. Soc. Photo-Optical Instrum. Eng.* 231:18
Schwartz, P. R. 1979. *Ap. J. Lett.* 229:L45
Schwartz, P. R., Bologna, J. M., Waak, J. A. 1978. *Ap. J.* 226:469
Schwartz, P. R., Cheung, A. C., Bologna, J. M., Chui, M. F., Waak, J. A., Matsakis, D. 1977. *Ap. J.* 218:671
Silk, J. 1980. In *Star Formation, 10th (SAAS-FEE) Adv. Course Swiss Soc. Astron. Astrophys.*, ed. I. Appenzeller, J. Lequeux, J. Silk, p. 131. Geneva: Geneva Obs.
Snell, R. L. 1981. *Ap. J. Suppl.* 45:121
Snell, R. L., Loren, R. B., Plambeck, R. L. 1980. *Ap. J. Lett.* 239:L17
Storey, J. W. V., Watson, D. M., Townes, C. H. 1980. *Int. J. Infrared Millimeter Waves* 1:15
Strom, K. M., Strom, S. E., Vrba, F. J. 1976. *Astron. J.* 81:320
Strom, S. E., Grasdalen, G. L., Strom, K. M. 1974. *Ap. J.* 191:111
Sweitzer, J. S. 1978. *Ap. J.* 225:116
Thompson, A. R., Clark, B. G., Wade, C. M., Napier, P. J. 1980. *Ap. J. Suppl.* 44:151
Townes, C. H., Genzel, R., Watson, D. M., Storey, J. W. V. 1983. Preprint
Townes, C. H., Schawlow, A. L. 1955. *Microwave Spectroscopy*. New York: McGraw-Hill
Turner, B. E., Zuckerman, B., Morris, M., Palmer, P. 1978. *Ap. J. Lett.* 219:L43

Turner, B. E., Zuckerman, B., Palmer, P., Morris, M. 1973. *Ap. J.* 186:123
Turner, J. L., Ho, P. T. P. 1983. *Ap. J. Lett.* In press
Ungerechts, H., Walmsley, C. M., Winnewisser, G. 1980. *Astron. Astrophys.* 88:259
Ungerechts, H., Walmsley, C. M., Winnewisser, G. 1982. *Astron. Astrophys.* 268:L79
Walmsley, C. M., Ungerechts, H. 1983. *Astron. Astrophys.* 111:339
Weinreb, S. 1980. *IEEE Trans. Microwave Theory Tech.* 28:1041
Wilson, T. L., Batrla, W., Pauls, T. A. 1982. *Astron. Astrophys.* 110:L20
Wilson, T. L., Bieging, J., Downes, D. 1978. *Astron. Astrophys.* 63:1
Wilson, T. L., Downes, D., Bieging, J. 1979. *Astron. Astrophys.* 71:275
Wilson, T. L., Pauls, T. 1979. *Astron. Astrophys.* 73:L10
Winnewisser, G., Churchwell, E., Walmsley, C. M. 1979. *Astron. Astrophys.* 72:215
Ziurys, L. M., Martin, R. N., Pauls, T. A., Wilson, T. L. 1981. *Astron. Astrophys.* 104:288
Zuckerman, B., Morris, M., Palmer, P. 1981. *Ap. J. Lett.* 250:L39